university of groningen / faculty of science and engineering / kapteyn astronomical institute

UNIVERSITY OF GRONINGEN

BACHELOR THESIS

Environmental dependence of the local Hubble constant

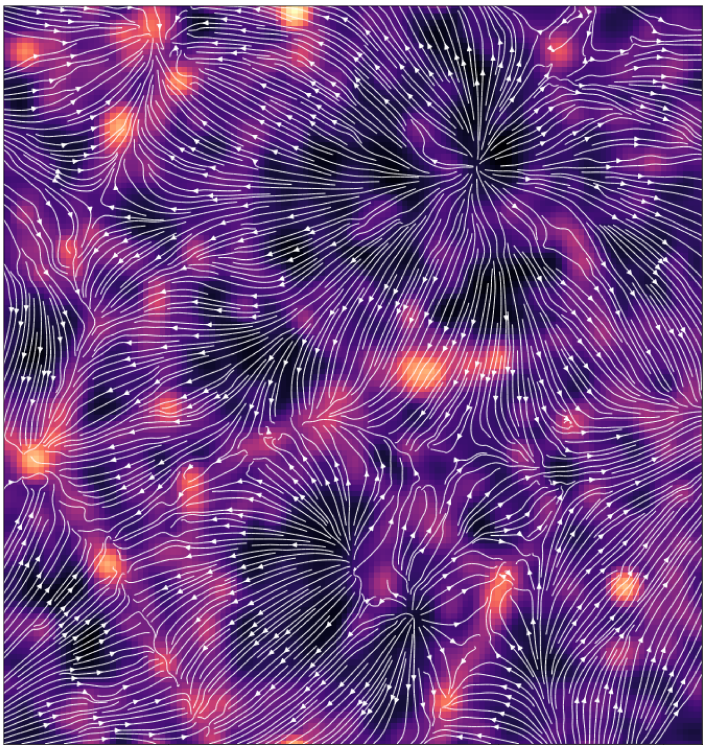

Author: Tetiana Ovramenko

Supervisor: prof. dr. Rien van de Weijgaert

Second examiner: prof. dr. E. Starkenburg

July 2024

Abstract

The value of the Hubble constant is of great significance in modern cosmology. Despite the large amount of solutions suggested to alleviate the Hubble tension, none of them seem to explain the discrepancy in the measurements fully. One of the assumptions suggests that a local underdensity might be a cause of a higher local Hubble flow. In this thesis, we are going to investigate the possible contribution of voids on the local Hubble constant in an effort to explain the deviation between early and late measurements of H_0. Using Watershed Void Finer on the Illustris simulation, we analyze the redshift distribution of dark matter particles and halos in the void regions. A dependence between the excess expansion rate and the size and depth of the voids was found. It was found that voids cannot fully explain the tension between local and global values of the Hubble constant.

Contents

1 Introduction **2**
1.1 Thesis Objective 4

2 Cosmological background **4**

3 On voids **6**
3.1 Void formation and evolution 7

4 Voids contribution to the excess expansion rate **7**
4.1 Voidfinding formalism 7
4.1.1 Illustris simulation: The data cube 7
4.1.2 Density cube: The Delaunay Tesselation Field Estimator 10
4.1.3 Identification of voids: The Watershed Void Finder 10
4.1.4 Void centers 14
4.1.5 Effective radii: Ellipsoidal fitting of voids 15
4.2 Lines of sight method 16

5 Results **18**

6 Discussion **23**

7 Conclusion **25**

References **26**

1 Introduction

One of the most important discoveries of the last century was made by Edwin Hubble in 1929 (Hubble, 1929). He presented the evidence for the expanding universe, making a cosmological breakthrough that changed our perception of the world and allowed us to start looking far beyond our Milky Way into the vast, deep universe. This conclusion comes from the famous graph of the distances to the nearby nebulae and their receding velocities that Hubble obtained from the 22 objects around the Milky Way (Figure 1), as further objects move away faster than the ones close by. The Hubble constant, H_0, is the slope of this linear relation; it represents the current expansion rate of the Universe. When the Hubble constant is known, the distance to any object in the Universe can be inferred easily by measuring only its radial component of the receding velocity.

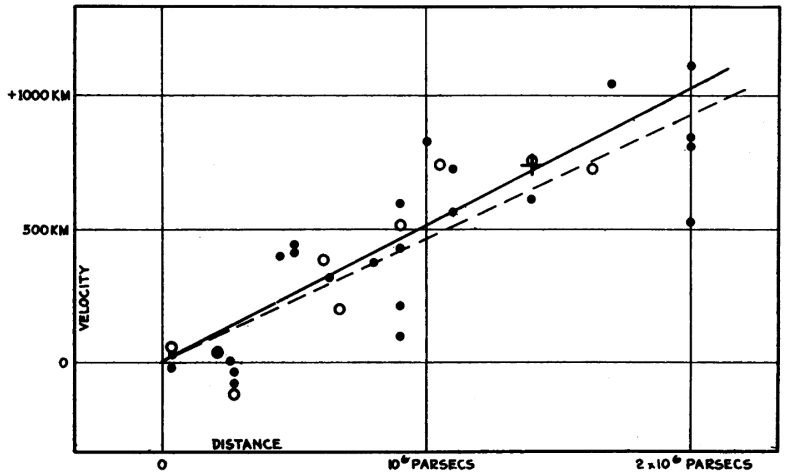

Figure 1: Velocity vs. distance relation for 22 nebulae nearby Milky Way (Hubble, 1929). Velocity was measured using shifts in the spectral lines of the nebulae spectra. Using Cepheids as standard candles, Hubble estimated the distances of these nebulae. The values of the Hubble constant that he obtained from the graph was $H_0 = 465 \pm 50$ km s^{-1} Mpc^{-1}, which implied that the Universe is only 2 Gyr old.

Since Edwin Hubble, the constant has been refined many times using various independent measurements. The most recent developments in this field reached a high level of precision. Despite this, there appears to be a discrepancy in the measurements due to the very different nature of the methods used to obtain them. Using the most recent data from the local distance, type Ia Supernovae the Cepheids, the Hubble constant is found to be $H_0^{\text{loc}} = 73.04 \pm 1.04$ km s^{-1} Mpc^{-1} (Riess et al., 2022), while measurements from the Cosmic Microwave Background (CMB) anisotropies give $H_0^{\text{CMB}} = 67.4 \pm 0.5$ km s^{-1} Mpc^{-1} (Planck Collaboration et al., 2020). The difference between these values is 8% (with 4.9σ confidence) when the error bars of the values (1.4% and 0.7% respectively) are much smaller. A difference of 5σ significance means that there is a 99.99994% chance that this discrepancy in the measurements is caused by some missing element in our perception of the Universe (*Why do physicists mention "five sigma" in their results? — CERN*, 2024).

There are many other means that allow the measurement of the Hubble constant, such as Tip of the Red Giant Branch (TRGB), lensed quasars, Baryon acoustic oscillations (BAO), megamasers, Surface Brightness Fluctuations (SBF), etc. Values extracted using these methods are shown in Figure 2 (Bonvin & Millon, 2020). In general, these methods could be divided into 2 groups: early and late Universe measurements, depending on the evolution stage of the data used in them. The inconsistency between the two approaches caused a discussion, which is known as the Hubble tension.

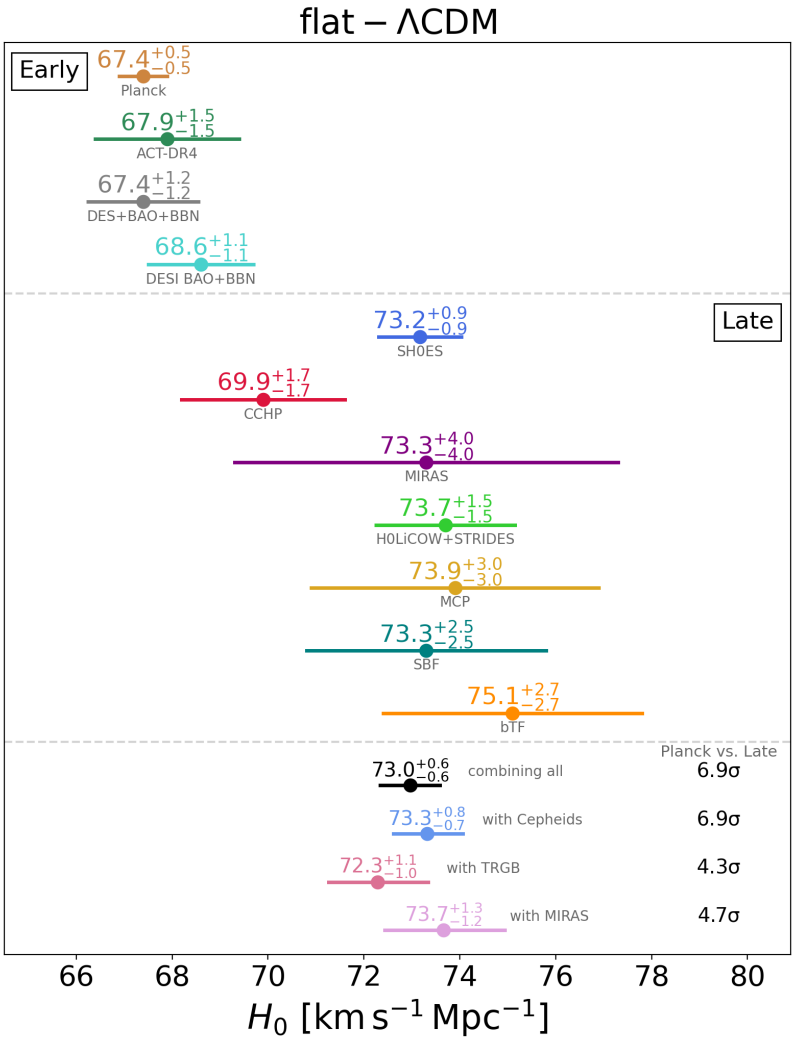

Figure 2: Compilation of Hubble Constant measurements taken from the most recent literature. Four measurements based on the data from the early Universe are shown at the top left. The middle part of the figure shows late Universe measurements. The bottom panel shows combinations of the late-Universe measurements and the respective tensions with the early-Universe predictions. The individual measurements shown on this plot correspond to the following references: 1. Planck (Planck Collaboration et al., 2020) - CMB observations; 2. ACT-DR4 (Aiola et al., 2020) - CMB observation from the Atacama Cosmology Telescope only; 3. DES+BAO+BBN (Abbott et al., 2018) - weak lensing, clustering, BAO, and BBN (Big Bang nucleosynthesis); 4. DESI BAO+BBN (DESI Collaboration et al., 2024); 5. SH0ES (Breuval et al., 2024) - distance ladder with SNe Ia and Cepheids; 6. CCHP (Freedman, 2021) - SNe Ia and TRGB; 7. MIRAS (Huang et al., 2020) - SNe Ia and Mira variables; 8. H0LiCOW+STRIDES (Wong et al., 2020) (Shajib et al., 2020) - lensed quasars; 9. MCP (Pesce et al., 2020) - megamasers; 10. SBF (Blakeslee et al., 2021) - SBF and Cepheids/TRGB; 11. bTF (Schombert et al., 2020) - baryonic Tully-Fisher relation with Cepheids and TRGB. In summary, the difference between measurements is more than 4σ. Illustration credit: (Bonvin & Millon, 2020)

There are dozens of possible explanations suggested in an effort to put the Hubble tension problem to an end, connecting the early and late Universe. (Di Valentino et al., 2021) gathered more than 1000 papers presenting various possible theoretical solutions developed over a decade. To the present moment, none of the suggested solutions have fully explained such a discrepancy in the values. Resolving the Hubble tension problem is of great importance to modern cosmology because it would connect observations and theory, which currently seems insufficient to explain all the aspects of cosmic evolution fully.

One of the simplest possible solutions to the tension implies that fluctuations in local density can change the expansion rate with respect to the global value due to the additional peculiar velocity component in the Hubble flow (Turner, Cen, & Ostriker, 1992) (Shi & Turner, 1998) (Fleury, Clarkson, & Maartens, 2017).

1.1 Thesis Objective

This work is focused on exploring a possible imprint of the void regions on the inferred value of the Hubble constant. A spatial analysis is performed on the cosmological simulation Illustris (Collaboration, n.d.) to measure the relative variations in the expansion rate depending on the density of the environment. To identify void structure within the simulation, the Delaunay Tesselation Field Estimator (DTFE) (Schaap, 2007) and Watershed Void Finder (WVF) (Platen, van de Weygaert, & Jones, 2007) formalisms were adopted. A method of lines of sight was used to infer a Hubble constant by performing a best-fit procedure for points within a specific direction from a void. The investigation is performed both on dark matter particles and subhalos to ensure the robustness of the analysis, as it would probe different scales of the simulation.

Our spatial analysis confirms the presence of a small effect of the local density fluctuations on the measurements of the local Hubble constant. Comparing this value to the global expansion rate of the simulation reveals its statistical significance.

2 Cosmological background

From the very first attempts to map the observable Universe, it was clear that the distribution of matter has a distinct structure known as the cosmic web (Chincarini & ROOD, 1975) (de Lapparent, Geller, & Huchra, 1986a) (Colless et al., 2001). The main components of the cosmic web are voids, nodes, filaments, and walls. The latter 3 are the overdense regions in the Universe separated by vast underdense voids. Voids are connected with each other by walls, whereas filaments are the edges between the walls. Nodes, or clusters, are the vertices within the structure of the Universe. Matter flows from voids into the walls and then via filaments into cluster regions (Cautun, van de Weygaert, Jones, & Frenk, 2014).

A map of the galaxy distribution is shown in Figure 3, where filaments and nodes are the regions of high concentration of galaxies, and voids are the empty regions between them. The typical scale of void sizes is $20 - 50h^{-1}$ Mpc (van de Weygaert & Schaap, 2009). They take up most of the volume in the Universe, though having the lowest mean density (Kugel, 2020). The fact that the matter distribution was mostly homogeneous, with small density perturbations, induced tidal forces that molded a large-scale structure as we see it now (van de Weygaert & Schaap, 2009). By analyzing the large-scale structure, we can investigate the formation and evolution of the Universe (Cautun et al., 2014), as well as estimate the cosmological parameters.

Hubble constant H_0 is the present-day value of the time-varying function $H(t)$ (Ryden, 2016). The Hubble parameter $H(t)$ is defined as

$$H(t) = \dot{a}/a, \tag{1}$$

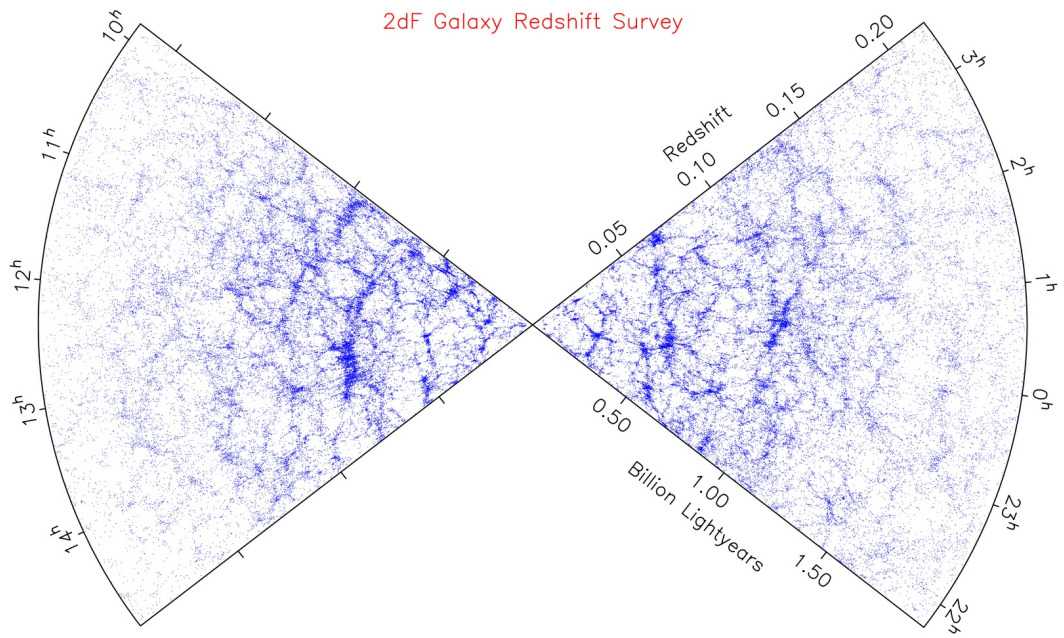

Figure 3: Redshift distribution of galaxies from 2dF Galaxy Redshift Survey obtained in 2001 (Colless et al., 2001). This survey determined the structure of the cosmic web in the directions of the north and south galactic poles up to a redshift of 0.2. Matter clumps together into filaments and nodes, making voids more prominent as they become emptier. Illustration credit: (*The 2dF Galaxy Redshift Survey*, n.d.)

where a is the cosmic scale factor, one of the parameters in the Friedmann equations, and $\dot{a}$ is its time derivative. Therefore, the Hubble constant is the Hubble parameter evaluated at the current moment in time:

$$H_0 = (\dot{a}/a)_{t=t_0}. \tag{2}$$

The scale factor is a dimensionless quantity, and by definition, $a_0 = 1$ is the present time value. If the Universe is expanding, it eventually leads to the fact that in the past, all the matter (and anti-matter) was together at one point, leading to the development of the Big Bang model (Alpher, 1999).

As mentioned before, Edwin Hubble discovered his famous relation in 1929, but he was not the first one to find this trend. In 1927, Georges Lemaitre published a paper in a small French journal proposing a model of an expanding universe in which he derived the velocity-distance relation before Hubble. His work got lost when translated into English, and therefore, his contribution was neglected for a very long time. Hubble's discovery was independent of Lemaitre and later by two years. In 2018, the Hubble law was renamed to the Hubble-Lemaitre law (*International Astronomical Union — IAU*, n.d.).

The Hubble-Lemaitre law is the relation between the distance from the observer to an object and its receding radial velocity as a result of the expansion of the Universe,

$$v = H_0 d, \tag{3}$$

where v is the recession velocity, H_0 is the Hubble constant, and d is the distance from the observer to the object.

The receding velocity of an object consists of the contribution due to the expansion of the Universe and also the peculiar motion of the galaxy that makes it deviate from the Hubble flow:

$$\vec{v} = H_0\vec{r} + \vec{v}_{\rm pec}, \tag{4}$$

where $\vec{v}$ is the observed velocity of the galaxy, H_0 is the Hubble parameter at the present moment, $\vec{r}$ is the position of the galaxy, and $\vec{v}_{\rm pec}$ is the peculiar velocity, the velocity of the galaxy with respect to the expansion of the Universe. Only a radial component is needed to proceed with the investigation:

$$cz = H_0 D + v_{r,\rm pec}, \tag{5}$$

where c is the speed of light, z observed redshift of the galaxy, D is distance from the observer to the galaxy, and $v_{r,\rm pec}$ is the radial component of the peculiar velocity. A non-relativistic version of the Hubble-Lemaitre law will be used, as the redshift distribution of the simulation is within very low values.

The variation of the local Hubble constant, $H_0^{\rm loc}$, according to theory, comes from the local fluctuations of the density,

$$\frac{\Delta H_0^{\rm loc}}{H_0^{\rm loc}} = -\frac{1}{3}\delta f(\Omega_M), \tag{6}$$

where $f(\Omega_M) \approx (\Omega_M)^\gamma$ in the flat ΛCDM Universe and $\gamma \approx 0.55$. For Ω_M adopted in the Illustris simulation, $f \approx 0.5$.

3 On voids

Since the conduction of the first galaxy surveys, it was noticed that the distribution of galaxies is not homogeneous on a certain scale, and there are regions that are almost devoid of any galaxies (Gregory & Thompson, 1978) (Einasto, Joeveer, & Saar, 1980). In 1981, Kirshner identified a large empty region in the galaxy distribution survey that he and his colleagues conducted (Kirshner, Oemler, Schechter, & Shectman, 1981), confirming it later (Kirshner, Oemler, Schechter, & Shectman, 1987) and calling it the Bootes void, a 60 Mpc sized void in the constellation Bootes (Figure 4).

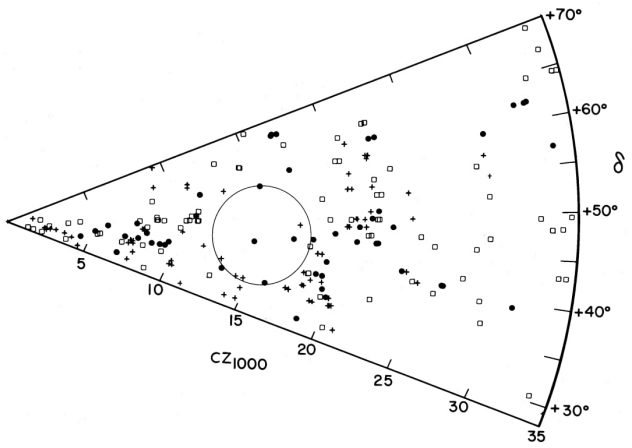

Figure 4: Distribution of galaxies in the velocity-declination space. The circle represents the Bootes void, drawn as the largest and emptiest circle that fits in that region (Kirshner et al., 1987).

From that moment, multiple surveys were conducted, each increasing in size over the years. They established the importance of voids in the large-scale structure of the Universe (de Lapparent, Geller, & Huchra, 1986b) (Colless et al., 2001) (Tegmark et al., 2004), and

the first method of void identification was developed (Hoyle & Vogeley, 2004) (Foster & Nelson, 2009).

3.1 Void formation and evolution

Small fluctuations in the primordial density and velocity field led to the creation of the large-scale structure. These density fluctuations with respect to the average density of the Universe are defined like

$$\delta(\vec{r}, t) = \frac{\rho(\vec{r}, t) - \rho}{\rho}, \tag{7}$$

where ρ is the mean density, and $\rho(r, t)$ is the density at a certain position $\vec{r}$ in space. These density fluctuations produce gravitational effects such that regions with higher than average density will attract more matter, and the future void regions become emptier (van de Weygaert & Bond, 2008). In return, The gravitational perturbations induce perturbations in the flow of matter, and as a result, voids become subject to the super-Hubble expansion, expanding faster than the background Universe (Sheth & van de Weygaert, 2004). The evolution of a isolated spherical void is shown in Figure 5. As a result of the super-Hubble expansion, matter evacuates from the center of the void, making it emptier with time. However, in reality, voids are not isolated since they are embedded in the cosmic web, where they interact with other surrounding voids.

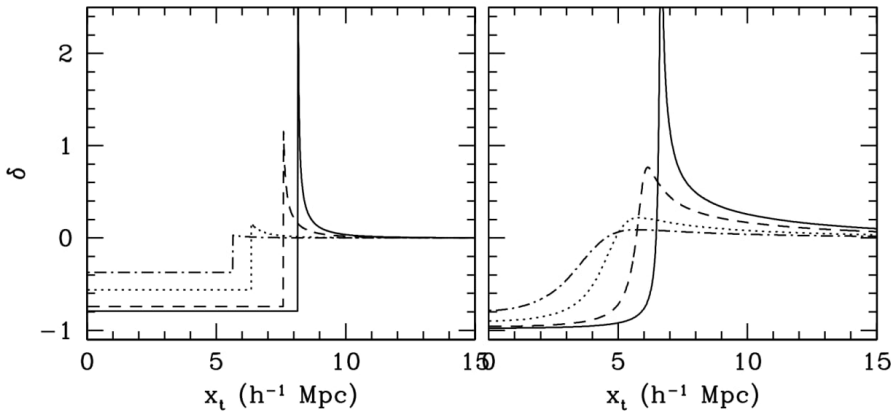

Figure 5: Evolution model for an ideal isolated spherical void. **Left:** Top-hat density profile model, where subsequent graphs represent time steps of the evolution process: top-hat function evolves into a "bucket-shape" profile. **Right:** Evolution of an angular averaged SCDM profile. In both cases, matter evacuates from the center towards the boundary of the void and forms a steep ridge. Illustration: (Sheth & van de Weygaert, 2004)

4 Voids contribution to the excess expansion rate

4.1 Voidfinding formalism

4.1.1 Illustris simulation: The data cube

For this project, we use the Illustris simulation, which is based on ΛCDM cosmology. Currently, ΛCDM cosmology is the favorite model for describing the evolution and structure of our Universe, and it is based on three major components. The cosmological constant Λ represents the amount of dark energy, which, discovered from the observations, prevails in the Universe. The second most abundant part is the cold dark matter (CDM), which is only

detectable because of its interaction with gravity. The baryonic (ordinary) matter is only a small fraction of all matter in the Universe. This model is considered the standard model of modern cosmology, as it is the most simple and stable model so far. The ΛCDM model is used to simulate the data cubes with dark matter particles and subhalos.

The difference between these two data cubes lies within a few factors. The dark matter particles model the distribution of the dark matter in the Universe, while subhalos are the distinct overdensities of these dark matter particles, gravitationally bound structures that form larger halos. Subhalos show the possible locations where galaxies might form, resembling a future galaxy distribution and uniting dark matter with visible one. they both probe different scales of the universe's structure, small and large, respectively.

The Illustris simulation uses parameters from WMAP-9 measurements (Hinshaw et al., 2013). The values for different cosmological parameters of this simulation can be seen in Table 1.

Parameter	Value
Dimensions	106.5 Mpc
Number of DM particles	455^3
Number of subhalos	111992
Total matter density Ω_M	0.2726
Dark energy density Ω_Λ	0.7274
Baryonic matter density Ω_b	0.0
Hubble constant H_0	70.4

Table 1: Details of the Illustris simulation

The value for the Hubble parameter used in this simulation is 70.4 km/s/Mpc. It is important to remember that for the analysis of the possible excess Hubble flow, we are not interested in the value itself but rather in its relative difference from the intrinsic Hubble parameter set in the simulation, in our case, $H_0 = 70.4$ km/s/Mpc. Therefore we adopt a concept of the deviation of the local Hubble constant:

$$\Delta H_0^{\text{loc}} = H_0^{\text{loc}} - H_0^{\text{true}} = H_0^{\text{loc}} - 70.4, \tag{8}$$

where H_0^{loc} is the local values of the Hubble constant and H_0^{true} is the global value of H_0 in the simulation.

The data cube is periodic with dimensions of 75 000 h^{-1} kpc (106.5 Mpc). We are using the snapshot of redshift $z = 0$ from Illustris-Dark-3: the simulation with only dark matter that has the lowest resolution (455^3 DM particles). Despite the fact that this is the lowest resolution, the amount of particles exceeds 94 million, which slows down the data processing significantly. A decision was made to take a random sample, decreasing the amount to 1 million points due to the strain on the system. Taking a sample from the data cube did not affect the results, as the structure within the cube was still well-recognizable: results of such sampling can be seen in Figure 6. However, when working with subhalos, the data cube contains only 111 992 particles, so there is no need to take a sample in this case (Figure 7). In both of these figures (Figures 6 & 7), the simulated large-scale structure can be recognized: filaments and nodes are the high-density regions (clumps of particles in blue), and the voids are the regions devoid of particles ("empty" regions).

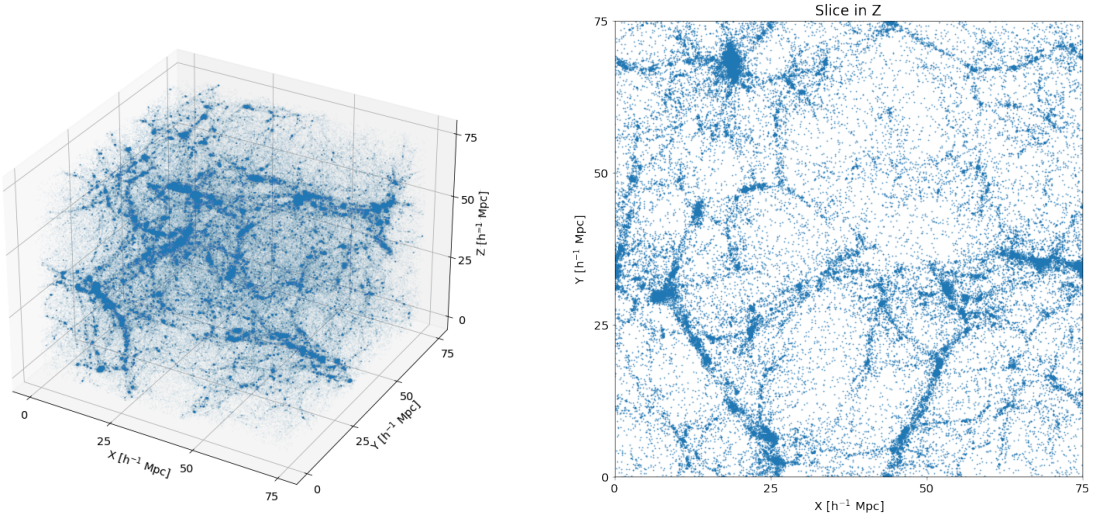

Figure 6: **Left panel:** Illustris-Dark-3 data cube of size 75 000 h^{-1} kpc (106.5 Mpc) with 455^3 dark matter (DM) particles. **Right panel:** slice of the data cube in Z direction with a thickness of 5 000 h^{-1} kpc.

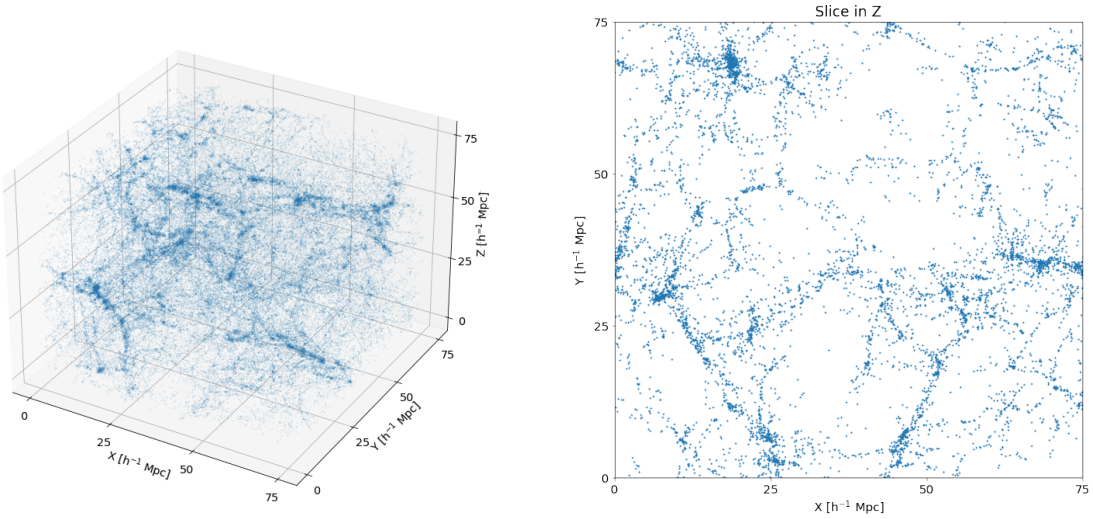

Figure 7: **Left panel:** Illustris-Dark-3 data cube of size 75 000 h^{-1} kpc (106.5 Mpc) with 111992 subhalos. **Right panel:** slice of the data cube in Z direction with thickness of 5 000 h^{-1} kpc.

Each particle in the cube has an ID, spatial position (in kpc/h), and spatial velocity (km/s) within the periodic box in 3 dimensions. For convenience, the position units were changed from kpc/h to Mpc, resulting in the cube's volume of 106.53 Mpc. This data cube is the basis of the results obtained in this thesis.

To produce a representative statistical analysis of the simulation, we need to identify all voids within the data cube. It can be done using the Watershed Void Finder (WVF), a procedure for identifying underdense regions (Platen et al., 2007). The WVF produces its output based on the continuous density field supplied. For this purpose, the Delaunay Tesselation Field Estimator (DTFE) was applied to the cube sample of data points from the simulation (Schaap, 2007). In this section, both of the algorithms will be presented.

4.1.2 Density cube: The Delaunay Tesselation Field Estimator

As the data cube from the Illustris-3 simulation is a particle distribution, it should be converted to a continuous density field. We apply the Delaunay Tesselation Field Estimator (DTFE) method to process the given sample of dark matter particle (or subhalo) positions from Illustris.

This method was developed by Schaap & van de Weygaert (Schaap, 2007) and is based on Delaunay tessellation of the distribution of particles: splitting space into mutually disjunct tetrahedra (no vertex lying inside the circumscribed sphere) (right panel of Figure 8). The inverse of the volume of the tesselation cells provides an estimated of the local density. The DTFE is able to fully show the substructure and anisotropies of the given discrete distribution, as well as reveal voids as uniform regions of low density.

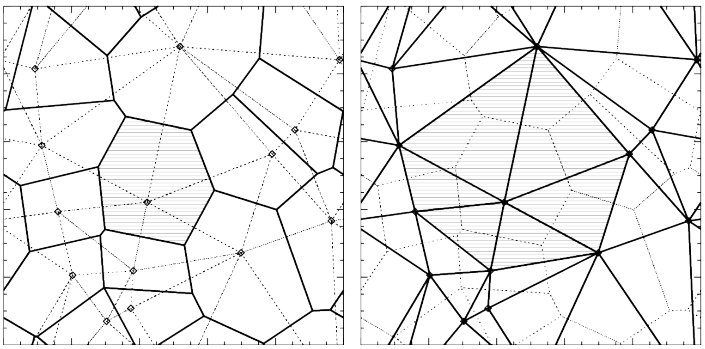

Figure 8: A set of points with their Voronoi (left panel) and Delaunay (right panel) tesselations. The center of each circumscribed sphere is a vertex of a Voronoi cell, and vice versa. (Schaap, 2007)

The final result of the DTFE is a field sampled on the grid of a certain size. A resolution of 128 x 128 x 128 is the most efficient, as it allows us to resolve the structure of the cosmic web at a reasonable level while requiring little computational power. This resolution was used to make maps of velocity streamlines, velocity divergence, and shear maps using code developed by Job Feldbrugge (Feldbrugge, 2021). However, a different code by Marius Cautun (Cautun, 2020) was used as input for the WVF, as it was compatible with it in terms of formats (no other difference in methods between these two options). For the application of the WVF method, the resolution of 256 x 256 x 256 was chosen , as the computing power allowed us to do so.

4.1.3 Identification of voids: The Watershed Void Finder

There is no set definition of a void, so their analysis is quite complicated, though it yields a lot of freedom. In this project, the Watershed Void Finder (WVF) was used to find voids in the data set for further investigation. This method was chosen as it does not make assumptions about the shape of the voids.

After the DTFE is applied to the data cube, the WVF could be used to find all void regions within the simulation sample. The Watershed Void Finder is chosen as the tool for void identification because of several advantages over other methods (Platen et al., 2007):

- No assumption is made on the shape of the voids: they can have any irregular shape.
- Ideally, the method is parameter-free: simply supplying a smooth density field is enough. In our case, a filtering radius (smoothing radius) needs to be supplied.
- Closed contours as the result of the procedure: this algorithm is not sensitive to bulges between neighbouring voids.

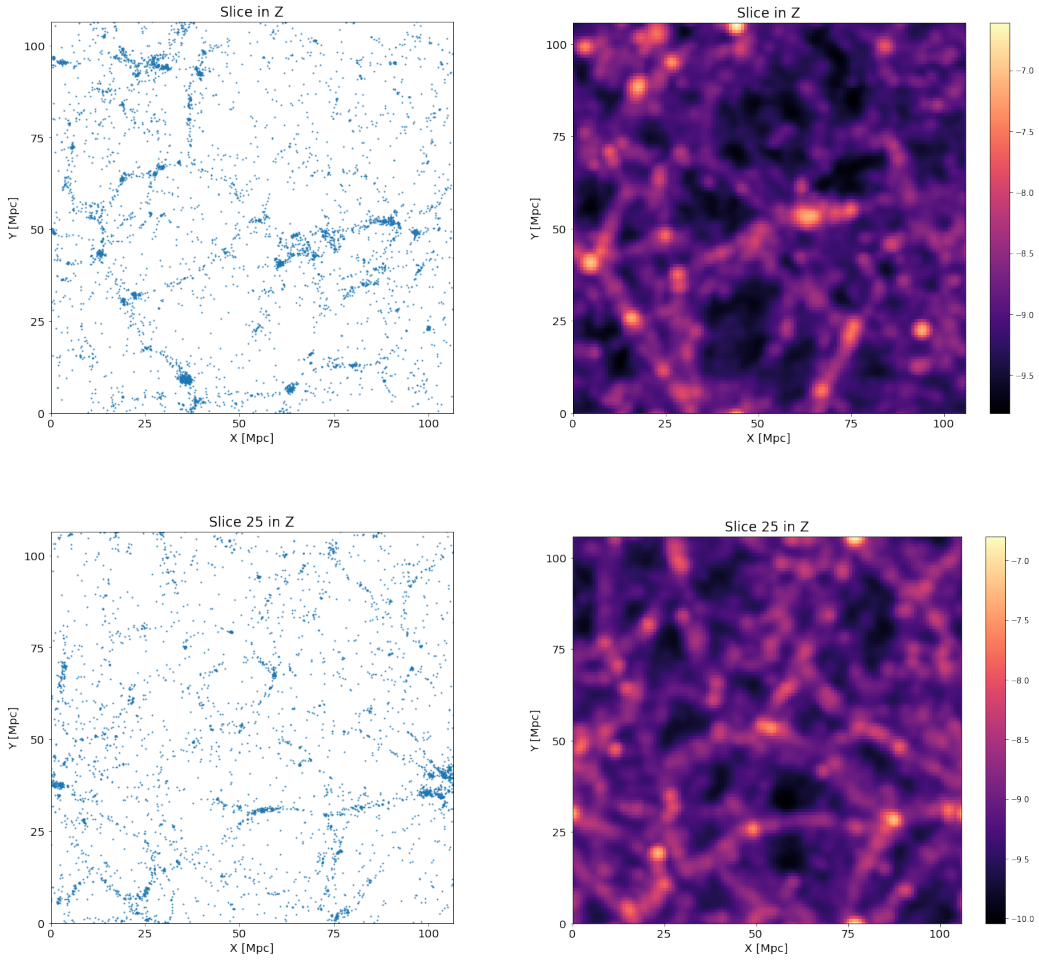

Figure 9: Examples of how the particle distribution is converted to a continuous density field by means of the DTFE method. The structure within the slices (on the left) is accurately represented in the resulting density field (on the right), where all the characteristic features of the cosmic web are observed: nodes (the bright spots), filaments (lines fainter than nodes connecting them) and voids (dark regions in between filaments). The scale of the color bar does not contain any physical meaning here. The results are produced using (Feldbrugge, 2021).

The Watershed Transform (WST) algorithm, which the WVF is based on, originates from the analogy with landscapes: marking boundaries of basins of rainfall collection. The algorithm of the WVF is the following:

1. Application of the DTFE for the conversion of the discrete particle distribution field to the continuous density field, which is then Gaussian smoothed.

2. The local minima of the DTFE density grid are found: points surrounded only by points with higher density values.

3. These points are the starting points of the "flooding" process: increasing density contour levels. Points are added to a specific basin if their density is lower than the current flooding level. When a point is reached by two neighboring basins, it becomes a boundary between them. This process is illustrated in Figure 10. In the cosmic web simulation, basins define void regions, and boundaries represent filaments and walls that separate the voids.

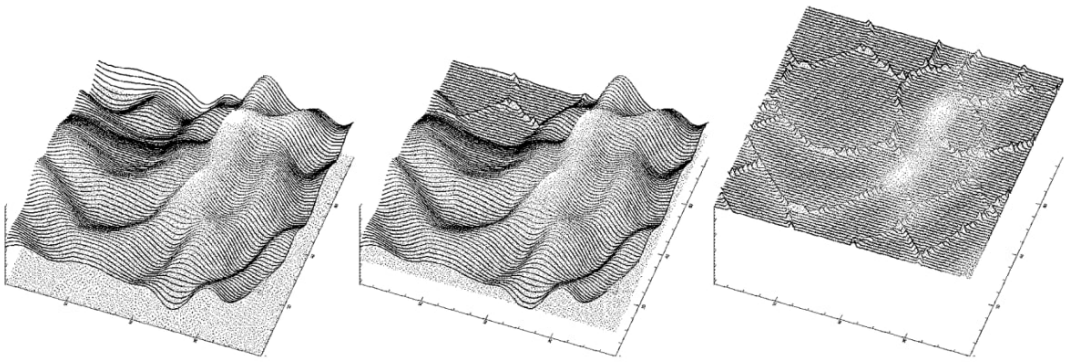

Figure 10: These frames show the main principle behind the Watershed Transform algorithm. The first frame from the left is the surface to be flooded. The plane below the surface represents the water level that is going to be rising. When the local minima are found, the flooding starts, and the water level rises, filling up the basins. The central frame shows how the ridges form as neighboring basins meet. The end result of the flooding process is a surface divided into segments separated by clearly defined boundaries (Platen et al., 2007).

The output of the Watershed is a grid, where each pixel has an ID that determines what void it belongs to. Therefore, this grid is sorted to extract pixel coordinates that belong to each void in the data box. The visual representation of this is shown in Figure 11, where a slice of a WVF grid is shown. Different voids can be easily distinguished, as they have different colors (do not carry any physical meaning). An example of a void in 3D, identified by the Wateshed procedure, and slices of it in 2D can be seen in Figure 12.

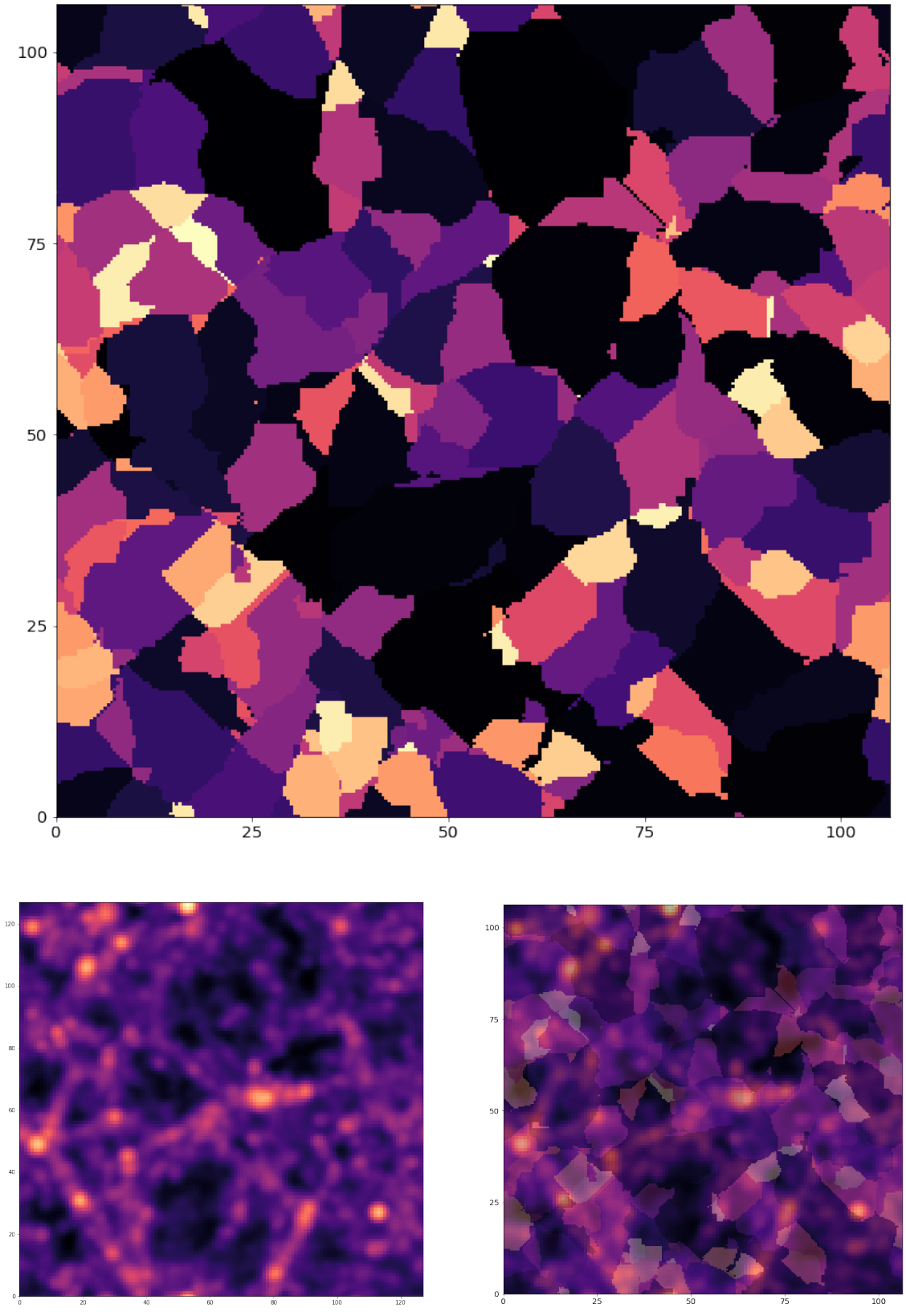

Figure 11: A slice (in the z-direction, where z=0) of a density field (bottom left panel), its corresponding slice in the WVF data cube with identified voids (top panel) and their overlap (bottom right panel). Different colors of the voids do not represent any physical property but are used to distinguish the voids in the data cube.

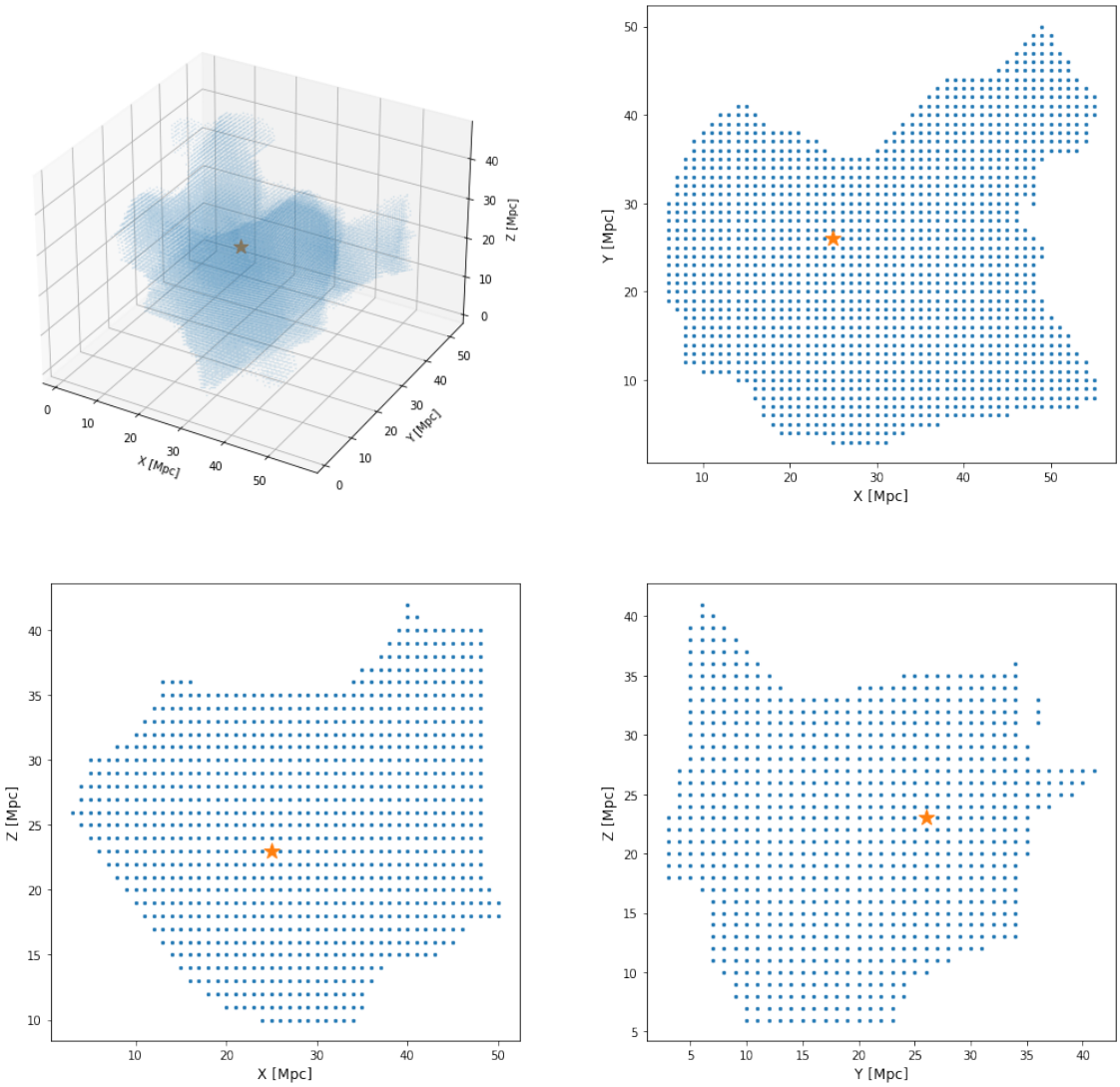

Figure 12: **Top left:** Void point distribution in 3D. The star represents the center of mass of the void. **Top right, bottom left & right:** Slices made through the center of the void in 3 planes, XY, XZ, and YZ respectively.

The grid obtained by means of the WVF procedure is used to determine the effective sizes of the voids and points of outflow to perform an environmental analysis of the Hubble flow in the simulation. The following sections describe the methodology for determining these quantities for further analysis.

4.1.4 Void centers

There is no classic method for determining the center of a void. Due to their irregular shapes, this becomes an issue. We introduce 3 different methods of determining the center of a void to obtain their shape characteristics within the simulation. One might think that the density minimum would be the most representable point, as it would be a characteristic point in the density profile of the void. Another option is to determine a barycenter, a mass (or density) weighted center of mass, as it would be the most classic approach for the overdense regions. A simpler method would be taking a mean value of the coordinates of all points belonging to the void. When looking at the velocity flow in the void region, a point of outflow is clearly visible, which could also serve as a characteristic center of the void. In

this project, we would try a few different approaches for determining void centers, as they might have an influence on the Hubble flow.

1. **Density weighted center of mass:** The most obvious way to evaluate an object's center is to compute its center of mass or barycenter using,

$$\vec{r}_{cm} = \frac{\sum_i \vec{r}_i \delta_i}{\sum_i \delta_i}, \tag{9}$$

where $\vec{r}_i$ is the position of a point on the grid within the void, δ_i is the density values at that point, which is technically a weight of that specific point. Due to the fact that density values range from -1 to any positive number, it is hard to apply normalization to these values. As a result of this method, in some cases, we get a center that is outside of the void or even outside of the data cube. This is caused by the overdensities on the edges of the voids, where density contrast reaches very high values. A threshold value of $\delta = 1$ was applied to the values of the density contrast. As a result, previously extreme values of centers do not affect the $\vec{r}_{cm}$ so much, allowing the estimated center point to be within the void volume.

2. **Density minimum as a void center:** Density values were taken from the Gaussian smoothed density field from the DTFE. The center was determined at the point of the lowest density contrast within the void,

$$\vec{r}_\delta = \vec{r}(\delta_{min}). \tag{10}$$

A theoretical density profile of a void looks like a top-hat model (Sheth & van de Weygaert, 2004), where the density within the void is uniform and doesn't have a clearly defined minimum. But in reality, there would be a minimum, which could be considered as the center of a void.

3. **Mean of the coordinates:** The most simple way to determine the center of the void is to compute the mean value of all the coordinates,

$$\langle \vec{r} \rangle = \frac{\sum_i \vec{r}_i}{N}. \tag{11}$$

In this case, the center will definitely be inside the void, unlike in the case of the center of mass. Though not the most physically accurate, it is the most trustworthy method of all.

4.1.5 Effective radii: Ellipsoidal fitting of voids

Approximating voids as ellipsoids is a very effective way of estimating their shapes. To fit an ellipsoid into a specific void, first, its center should be identified by means of one of the 3 above-described methods. The origin should be relocated to the center of the void. It is done to make all the points have coordinates as vector positions with respect to the void center. After that, a covariance ellipsoid is fitted. By doing this, eigenvalues of the covariance matrix of the data are found: they contain information about the size of the fitted ellipsoid - its semi-axes. The code by (Beeftink, 2019) was generalized in 3 dimensions and used to make these fits. As a result, principal semi-axes of the ellipsoids were determined. Periodic conditions were taken into account in order to receive information for all the voids within the simulation data cube. This is described n more detail in (Beeftink, 2019) as well.

As voids have very irregular shapes, it is hard to give a definition of the radius of a void. In this project, a way to characterize the effective size of a void was implemented from (Bos,

van de Weygaert, Dolag, & Pettorino, 2012), where they calculate the effective radius of the void as

$$r = \sqrt{abc}, \tag{12}$$

where a, b and c are the semi-axes of the fitted ellipsoid.

4.2 Lines of sight method

Knowing the coordinates of the centers of all voids in the data cube allows us to position the observer inside them and measure the Hubble constant for each void. Therefore, for each individual void, the cube's origin was shifted to be in the center of the void, whether it is the barycenter, mean, or density minimum. From this point of view, the radial component of the velocity vector is calculated for each point in the data cube using

$$v_r = \frac{\vec{v} \cdot \vec{r}}{r}, \tag{13}$$

where $\vec{v}$ is the velocity vector and $\vec{r}$ is the position vector of a particle, and r is the distance from the observer to the particle.

Due to the contribution of the peculiar velocities to the total radial recession velocity of the particles, we need to limit the number of particles in the radial direction by taking a lower limit on the distance from the center of the void. Therefore, we implement a 10 Mpc limit within the cone of light of sight, as the impact of peculiar velocities becomes minimal.

For further convenience, the coordinates are transformed from cartesian (x, y, z) to spherical (r, α, δ). To make all lines of sight equal in length, we should cut the cube into a sphere. The initial size of the cube is 106.5 Mpc, so the radius for the sphere was chosen to be 53 Mpc, which almost reaches the edges of the initial data cube. Then, a slice in the declination space is taken from $-1.5°$ to $1.5°$. The slice itself is divided into sectors of $3°$ in the dimension of right ascension. As a result of such cuts, we get 120 cones (technically, very thin pyramids) representing our future lines of sight. The size of these cones is chosen in a way, so that the points lie close enough to each other to be considered within one line of sight. Figure 13 illustrates this process. The ratio of the radius of the cone to its height is 0.08.

For each point in the sphere, the total velocity is calculated as

$$v = cz = H_0 r + v_r = \tilde{H} r_{pec} \tag{14}$$

,

where $H_0 = 70.4$ km/s/Mpc, the Hubble parameter defined in the simulation, r is the distance to the particle from the observer and v_r is the peculiar velocity of the particle found from Equation 13.

As we know both the velocities and distances of the particles with respect to the observer, we can fit the data to the Hubble law to get an estimate of the Hubble parameter. Using Least Squares Method, we fit the data to a function with only one free parameter:

$$v = \tilde{H} r, \tag{15}$$

where $\tilde{H}$ is the Hubble constant that contains the peculiar velocity of the particle due to the void expansion.

An important detail to consider when fitting data from cones is that the part of the cone closer to the observer would contain fewer points than the end of the cone at the ridge of the sphere. Therefore, it is important to introduce weights here. The amount of points in the specific shell of the cone depends on the distance from the center, so reasonable values

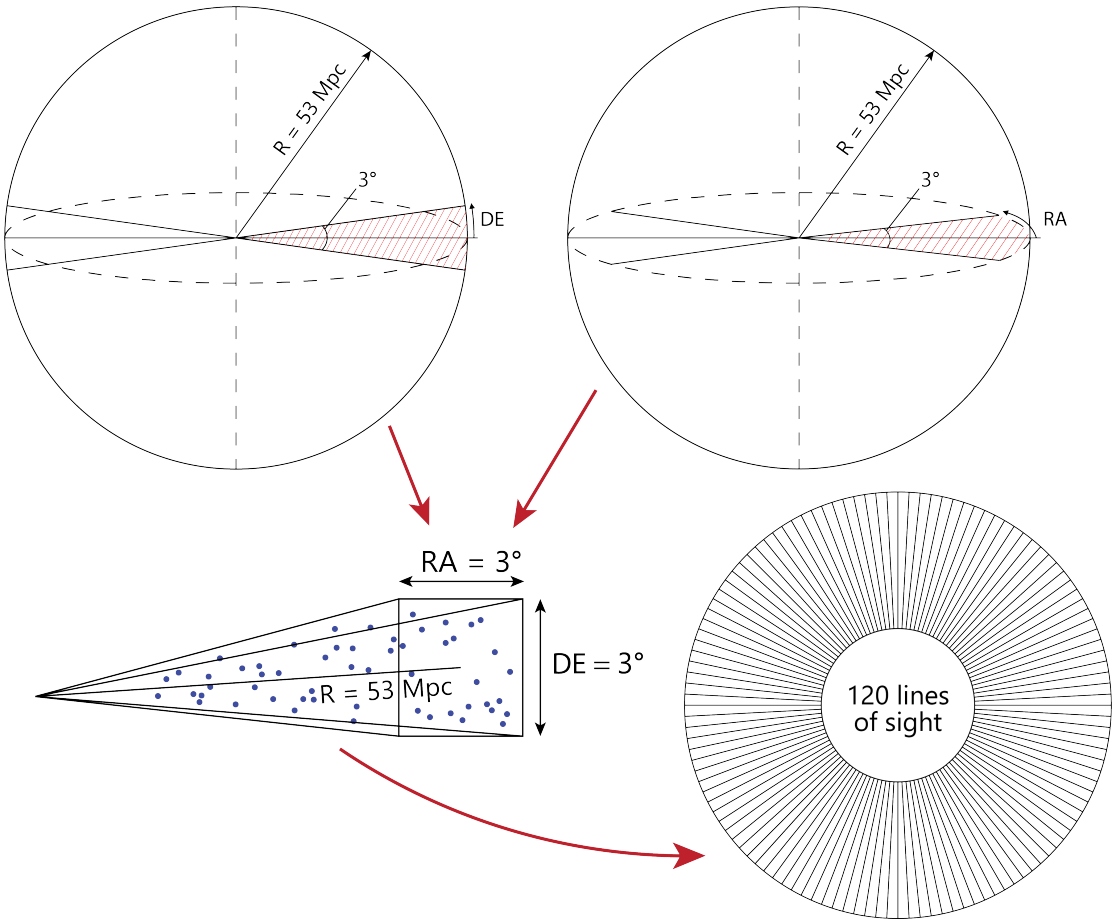

Figure 13: Illustration explaining method of lines of sight. When the origin is shifted to the center of the void, the coordinates are converted from cartesian to spherical and a sphere of $R = 53$ Mpc is cut out from the data cube. A slice in the declination space is cut, such as DE $\in [-1.5°; 1.5°]$. This slice is divided into 120 segments in the right ascension space, resulting in 120 spherical segments with a square base dimension of 3°. Points within that segment are used to determine H_0 for the specific line of sight.

for the weight of the point would be a normalized distance to the observer as it would be in the range of $[0, 1]$.

The fit should provide a good estimate of the inferred Hubble constant and a corresponding error for a specific line of sight. From one slice in the declination space, we get 120 lines of sight. To estimate a characteristic Hubble parameter for a void, we take a weighted mean

$$\bar{H}_0 = \frac{\sum_i H_{0i} w_i}{\sum_i w_i}, \tag{16}$$

where H_{0i} is the Hubble constant of a single individual line of sight within the slice and $w_i = 1/\sigma_i^2$ is the inverse of the variance of the specific H_{0i}. The error on the weighted mean is calculated like

$$\sigma_{\bar{H}_0} = \sqrt{\frac{1}{\sum_i \sigma_i^{-2}}} = \sqrt{\frac{1}{\sum_i w_i}}. \tag{17}$$

As a result, we can determine the distribution of the Hubble constant for all voids in the simulation box.

5 Results

Examples of plots for some line-of-sights within one void can be seen in Figure 14. A value for the Hubble constant is determined in every direction from the inside of the void, where it is defined as the slope of the fit to the data points. Weights of the inverse distance are implemented to take into account the sampling bias due to the shape of the line-of-sight segments.

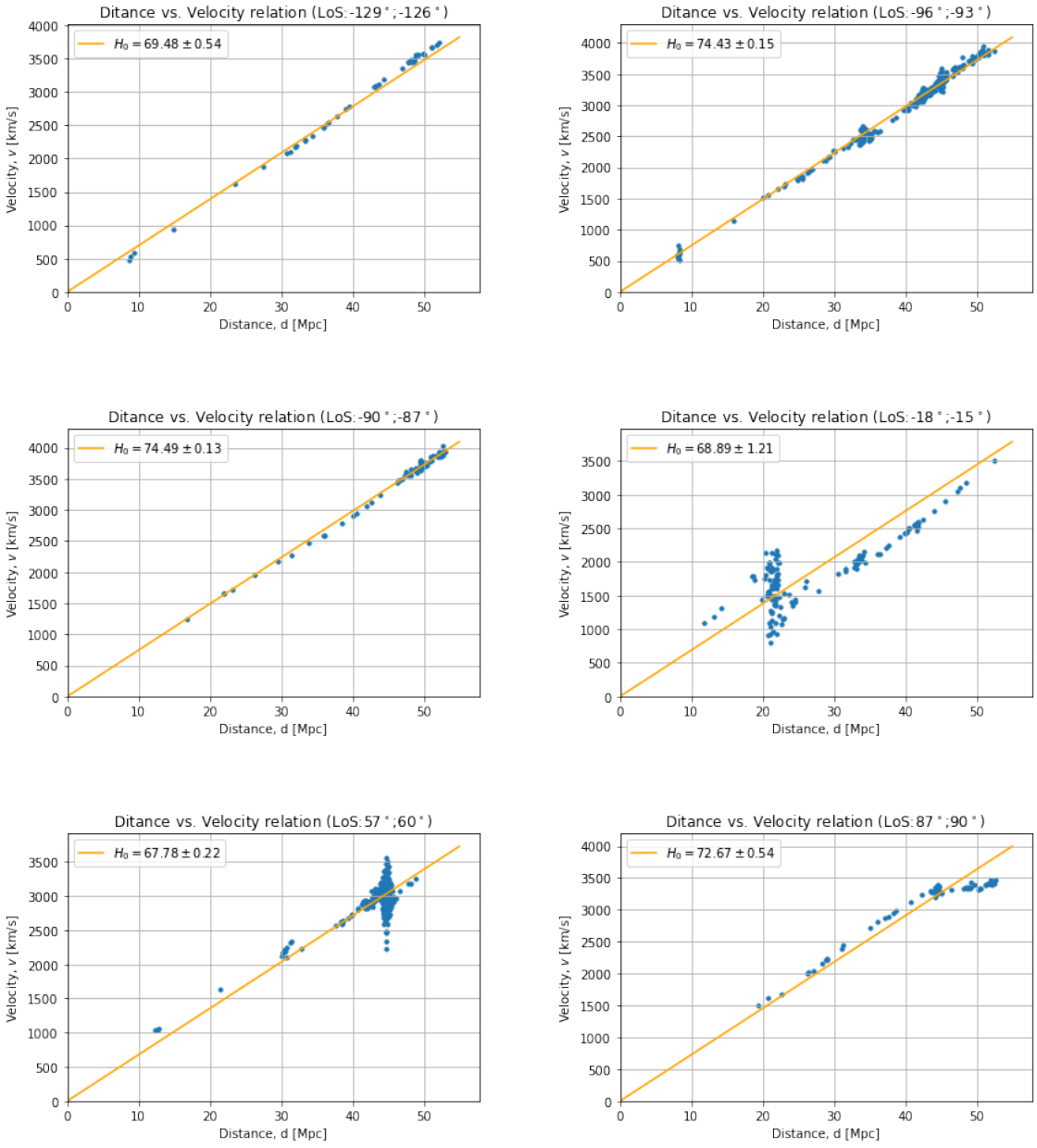

Figure 14: Examples of line-of-sight fits: distance to the particle is plotted versus v_{pec}, where the slope of the line is the Hubble constant in that specific direction. The slope is determined by fitting a line through the points using the Least Squares method. As the structure farther away in the spherical segment is more heavily sampled, distance-related weights $(1/r^2)$ were implemented on each point to prevent overfitting of these data points. The vertical structure in the plots represents a cluster within the line of sight.

Using the line-of-sight method for the full sample of voids found within the data cube,

we obtained histograms corresponding to different methods of determining centers of voids. Figure 15 shows the distribution of the local Hubble constant from the inside of the void sample for dark matter particles distribution, whereas Figure 16 depicts the same, but for the subhalos. Each histograms contains 1215 data points, as it is the amount of voids found within the data cube.

The weighted mean was estimated for each distribution using Equation 16, where the error determined is the weighted mean error from Equation 17. The standard deviation is determined for each distribution, as it would be the most representative error on the weighted mean (Table 2). Therefore, the final values resulting from the histograms are the weighted mean with the standard deviation of the distribution. The significance of the results is estimated as

$$\sigma = \frac{H_0^{\text{loc}} - H_0^{\text{true}}}{\sqrt{\sigma_{\text{loc}}^2 + \sigma_{\text{true}}^2}}, \tag{18}$$

where $H_0^{\text{true}} = 70.4$ km s^{-1} Mpc^{-1}. Significance is used as the way to tell if the result is significantly relevant and is able to cover the range of differences that cause the Hubble tension.

Type of center	Weighted mean	Standard deviation	Result	Significance
Particles				
Barycenter	70.945 ± 0.005	1.581	70.9 ± 1.6	0.35
Density Minimum	70.931 ± 0.005	1.591	70.9 ± 1.6	0.35
Mean	70.886 ± 0.005	1.619	70.9 ± 1.6	0.3
Subhalos				
Barycenter	71.114 ± 0.005	1.690	71.1 ± 1.7	0.4
Density Minimum	70.988 ± 0.005	1.658	71.0 ± 1.7	0.35
Mean	71.086 ± 0.005	1.698	71.0 ± 1.7	0.4

Table 2: Results from the statistical analysis of the distribution of the local Hubble constant in the underdense regions. Values are found for DM particle and subhalo data samples.

To proceed with the environmental investigation of the void impact on the Hubble flow, we inspect if there is any dependence between the void sizes and their depth. Effective radii of the voids are found using centers as the mean of the coordinates. Density contrast is determined as the average density within the effective radius of the void. This relation can be seen in Figure 17, which resembles the result of (Nadathur et al., 2015) as expected. The scatter in this plot is inherent due to the interactions between voids. However, the trend is still clear: larger voids tend to be deeper than the smaller ones.

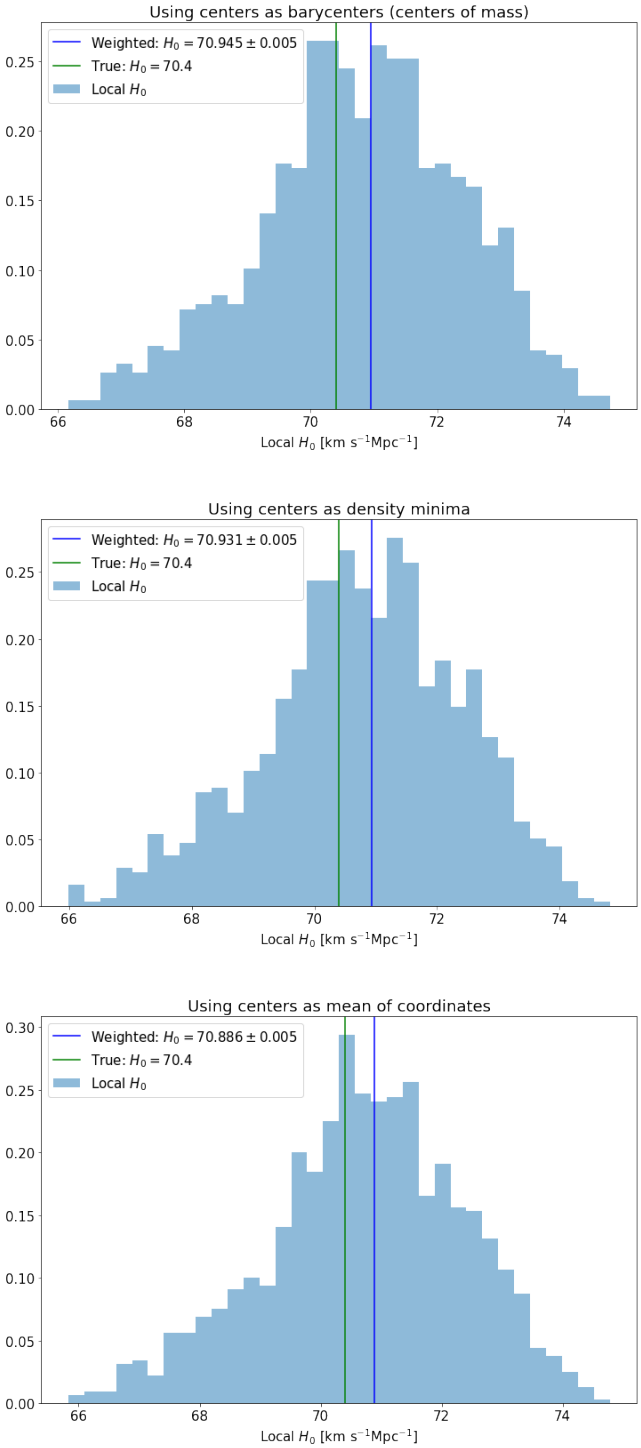

Figure 15: Histograms of the distribution of the local Hubble constant inferred from the underdense regions in the simulation using 3 different methods to find the center of such region. **Top:** Centers are determined at the center of mass of the voids. **Middle:** Centers are determined as the density minima within the void region. **Bottom:** Centers are the mean of the coordinates of the points that belong to one void. All histograms include the weighted mean of the distribution, compared to the global value of $H_0 = 70.4$ km s^{-1} Mpc^{-1}. Distributions are drawn from the dark matter particle data cube.

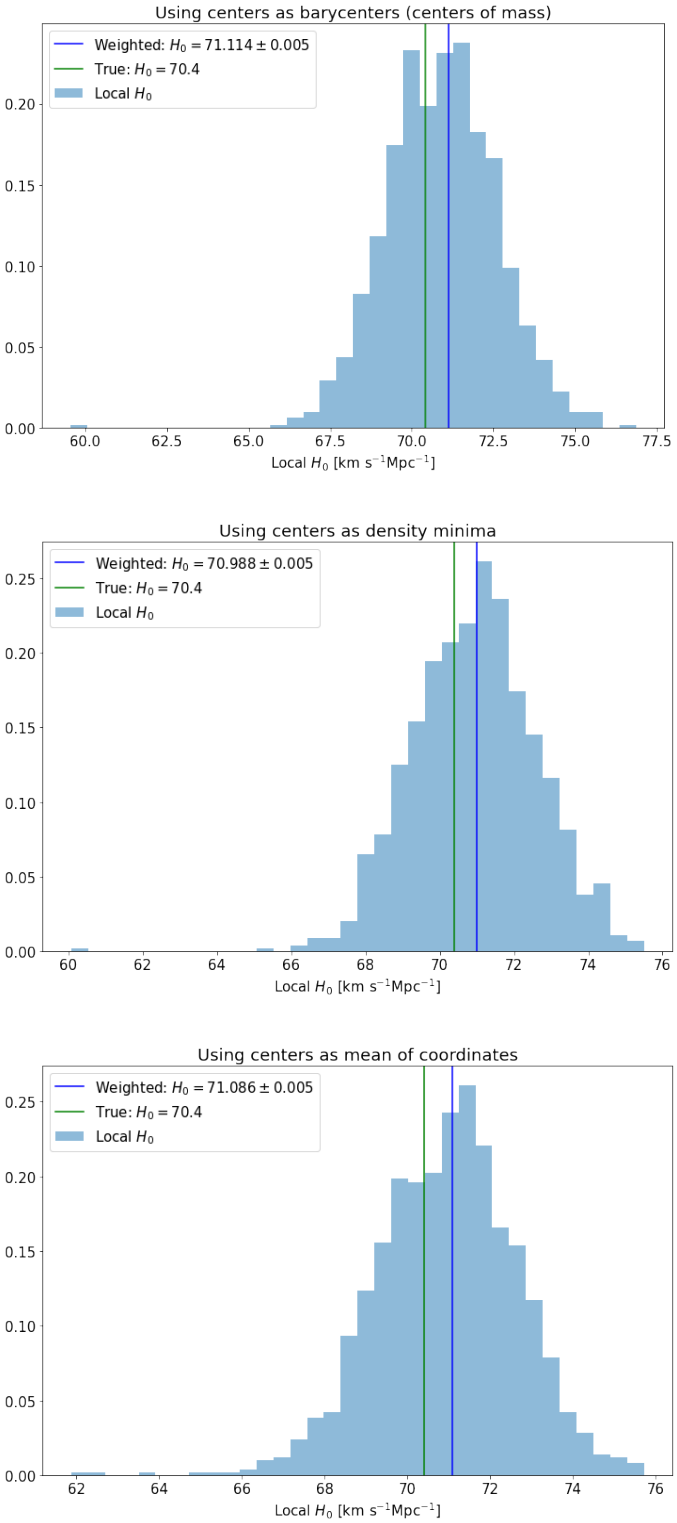

Figure 16: Histograms of the distribution of the local Hubble constant inferred from the underdense regions in the simulation using 3 different methods to find the center of such region. **Top:** Centers are determined at the center of mass of the voids. **Middle:** Centers are determined as the density minima within the void region. **Bottom:** Centers are the mean of the coordinates of the points that belong to one void. All histograms include the weighted mean of the distribution, compared to the global value of $H_0 = 70.4$ km s^{-1} Mpc^{-1}. Distributions are drawn from the subhalos data cube.

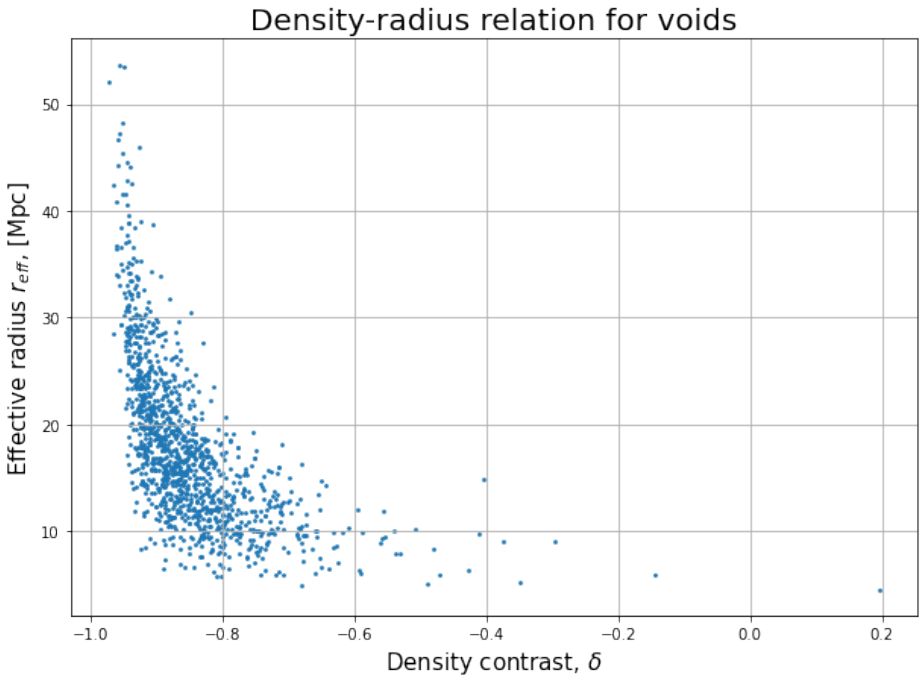

Figure 17: Correlation between density contrast in the central part of the void and its effective radius. A high level of scatter is inherent in this case because of the mutual interaction of voids in the distribution. The relation matches the one in (Nadathur et al., 2015).

In (Wu & Huterer, 2017), the observations show that this difference can be reached at $\delta \approx -0.8$, with radius of 120 h^{-1} Mpc, which is a large and deep underdense region that is very unlikely in the ΛCDM Universe. However, the fact that such a void could alleviate the tension is a possibility. Recent studies have explored the idea that under-/overdense regions can be the cause of the deviation of the local Hubble constant from the global value (Kenworthy, Scolnic, & Riess, 2019), (Mazurenko, Banik, Kroupa, & Haslbauer, 2024), (Giani, Howlett, Said, Davis, & Vagnozzi, 2024). As the local structure produces large inflows or outflows of matter, it is important to take this bias into account. The study by (Kenworthy et al., 2019) has shown that the change in the Hubble constant due to the fluctuation of the density is only around 2.2%, which does not have an influence on the discrepancy. However, in their research, the data used goes up only to a redshift of 0.5, whereas the evidence of the local void is found to be at higher redshifts. (Giani et al., 2024) have found that the Laniakea, a supercluster hosting the Milky Way, increases the Hubble tension by producing negative average expansion, whereas (Mazurenko et al., 2024) showed that the large local KBC void (Keenan, Barger, & Cowie, 2013) produces outflows that change the local bulk flow (on a smaller scale than the flow of the Local Group) that give rise to the decrease in the discrepancy between the Plank and SH0ES measurements. This explains both the Hubble tension and the existence of a very unlikely KBC void in the ΛCDM Universe. In (Wu & Huterer, 2017), the observations show that this difference can be reached at $\delta \approx -0.8$, with radius of 120 h^{-1} Mpc, which is a large and deep underdense region that is very unlikely in the ΛCDM Universe. However, the fact that such a void could alleviate the tension is a possibility. Recent studies have explored the idea that under-/overdense regions can be the cause of the deviation of the local Hubble constant from the global value (Kenworthy et al., 2019), (Mazurenko et al., 2024), (Giani et al., 2024). As the local structure produces large inflows or outflows of matter, it is important to take this bias into account. The study by (Kenworthy et al., 2019) has shown that the change in the Hubble constant due to the fluctuation of the density is only around 2.2%, which does not

have an influence on the discrepancy. However, in their research, the data used goes up only to a redshift of 0.5, whereas the evidence of the local void is found to be at higher redshifts. (Giani et al., 2024) have found that the Laniakea, a supercluster hosting the Milky Way, increases the Hubble tension by producing negative average expansion, whereas (Mazurenko et al., 2024) showed that the large local KBC void (Keenan et al., 2013) produces outflows that change the local bulk flow (on a smaller scale than the flow of the Local Group) that give rise to the decrease in the discrepancy between the Plank and SH0ES measurements. This explains both the Hubble tension and the existence of a very unlikely KBC void in the ΛCDM Universe. Now, we can investigate the relation between the deviation of the local Hubble constant and the density perturbations (Equation 7). Theoretically, a higher local expansion rate is expected when the density contrast is negative, as was shown previously in Equation 6. These relations are depicted in Figure 18 for both dark matter particles and subhalos, where they are compared to the tension between the Planck and SH0ES measurements of the constant.

6 Discussion

After applying the standard deviation from the distribution to the weighted mean, the resulting value can be seen in the 4th column in Table 2. All three methods of evaluating the center of the void arrive at the same result as they lie within the 1σ. Therefore, no difference between these methods will be drawn in this discussion. The investigation was important because it was important to examine the influence of the center estimation, as it might influence the Hubble flow. However, a further more precise analysis could be made to inspect the difference between using these methods.

The global value of the Hubble constant in the simulation, $H_0^{\text{true}} = 70.4$ km s^{-1} Mpc^{-1}, lies within 1σ of the obtained values from the histograms. However, the weighted mean values of all the distributions are confidently higher than the true value for both the DM particles and subhalos. This effect might be confirmed with a greater certainty in a few ways.

Looking at the histograms for the DM particles (Figure 15), we can see that the distribution is skewed to the left, with a more flat but bigger left wing. When investigating the Hubble law individual fits in more detail (as in Figure 14), it was noticed that a lot of significant local structure influences the fit by a substantial amount, producing low values of the Hubble constant. Extremely local overdensitites with high dispersion in the peculiar velocity produce ovefitting problems. We tried to avoid it by setting a lower limit to the distance of the particles within the ligh-of-sight segment, which improved the distribution significantly. Therefore, an assumption was made that the low values in the flatter wing can come from the collapsing voids (Sheth & van de Weygaert, 2004). As the voids is pushed from the outside by the overdense regions surrounding it, the expansion rate can become lower than the global value. This is a very intriguing assumption, that definitely should be looked into. Excluding such voids from the distribution can shift the weighted mean to higher values improving the significance of the result and accounting for more difference of the Hubble tension.

The H_0 distribution from the dark matter particle data cube seem to have 2 prominent peaks: one around the true value and another one at a higher values, implying that it is statistically possible to have a higher chance of determining a higher values of the local expansion rate. The values from the subhalo distribution are peaking at values close to the weighted mean, rather than the global values, confirming the result with even greater significance, as bigger part of the distribution lies to the right of the $H_0^{\text{true}} = 70.4$ km s^{-1} Mpc^{-1}.

Significance of the obtained result varies between 0.3σ and 0.4σ, whereas the tension between the Plank and SH0ES measurements reaches 4.9σ confidence level. Therefore, it

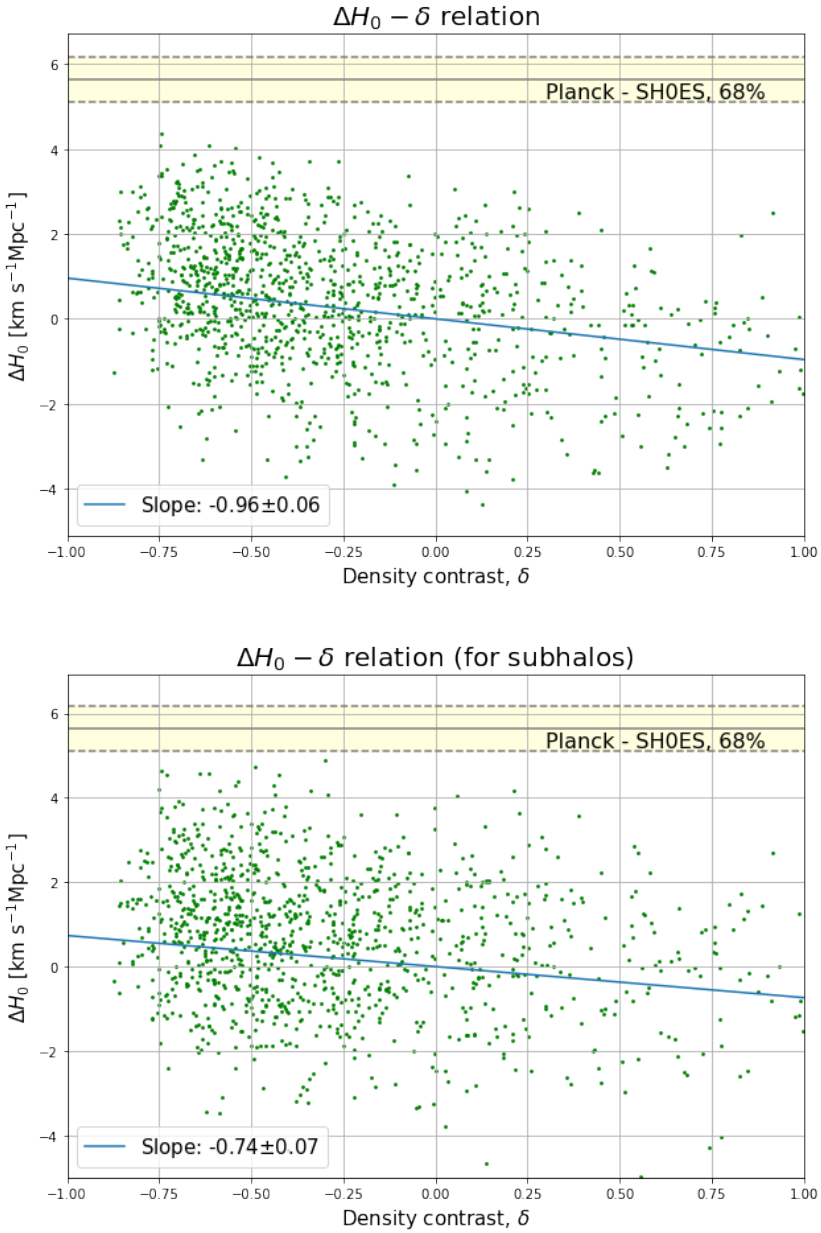

Figure 18: Deviation of the local Hubble constant as a function of the density contrast for DM particles and the subhalos. Each point represents a deviation of the $H_0^{\rm loc}$ from the global value in the specific void in the cube with respect to the average density contrast in that void. Using the Least Squares method, the fit was made through all the points. 1σ difference range between the Plank and SH0ES measurements of the Hubble constant is depicted to estimate the possible contribution of the voids to the tension.

is hard to conclude that local underdesity can alleviate the Hubble tension. Although is is clear that there is definitely an environmental dependence of the local expansion rate. This can be also seen more clearly in Figure 18. According to theory, a slope of 0.167 is expected, which does not lie within the statistically significant confidence level of our values.

Density contrasts of all order are present in the distribution, sampling the range effectively to be able to draw conclusions. The level of scatter in the distribution is significant, but a general downward is definitely present, as predicted by theory. For the dark matter particle data cube, voids can account only for the 0.96 km s^{-1} Mpc^{-1} difference between the global and local values when the tension between late and early universe measurements reach 6 km s^{-1} Mpc^{-1} difference. For the subhalo data sample, this value is even smaller.

In (Wu & Huterer, 2017), the observations show that this difference can be reached at $\delta \approx -0.8$, with radius of 120 h^{-1} Mpc, which is a large and deep underdense region that is very unlikely in the ΛCDM Universe. However, the fact that such a void could alleviate the tension is a possibility. Recent studies have explored the idea that under-/overdense regions can be the cause of the deviation of the local Hubble constant from the global value (Kenworthy et al., 2019), (Mazurenko et al., 2024), (Giani et al., 2024). As the local structure produces large inflows or outflows of matter, it is important to take this bias into account. The study by (Kenworthy et al., 2019) has shown that the change in the Hubble constant due to the fluctuation of the density is only around 2.2%, which does not have an influence on the discrepancy. However, in their research, the data used goes up only to a redshift of 0.5, whereas the evidence of the local void is found to be at higher redshifts. (Giani et al., 2024) have found that the Laniakea, a supercluster hosting the Milky Way, increases the Hubble tension by producing negative average expansion, whereas (Mazurenko et al., 2024) showed that the large local KBC void (Keenan et al., 2013) produces outflows that change the local bulk flow (on a smaller scale than the flow of the Local Group) that give rise to the decrease in the discrepancy between the Plank and SH0ES measurements. This explains both the Hubble tension and the existence of a very unlikely KBC void in the ΛCDM Universe.

Recently, the data from the JWST telescope was used to determine the local value of the Hubble constant using the cosmic distance ladder method (Li et al., 2024). The result yields a value of $H_0 = 74.7 \pm 2.1$ km s^{-1} Mpc^{-1}, producing a slight increase in the discrepancy of the early and late universe measurements. Although the results are new and waiting to be refined even more, this puts our perspective of the evolution of the Universe under doubt.

7 Conclusion

In this thesis, we investigated the influence of the underdense regions on the discrepancy between the measurements of the local and global values of the Hubble constant. Using cosmological simulation Illustris, we were able to explore this dependence on two data sets, with dark matter particles and subhalos, in order to probe a different scale of gravitationally bound structures. The Watershed Void Finder was used for the identification of voids in the data cube, as this method does not make an assumption about the shape of voids. A method of lines of sight was implemented in order to gather statistical data from each individual void.

Analysis of this data revealed the expected behavior of the expansion rate, although it did not show signs of being able to explain the existing tension fully. The variations of the local Hubble constant in the underdense regions are present but fail to connect early (Riess et al., 2022) and late (Planck Collaboration et al., 2020) universe measurements. This implies that, while voids have an effect on the dynamical properties of the Universe, the solution to the Hubble tension lies somewhere else.

The method of taking lines of sight could be further refined to increase the confidence in this study's results. This work contributes to the continuous search for the solution of the Hubble tension. By understanding and quantifying the dynamical influence of voids on

the expansion rate, we are able to confirm the importance of the underdense regions in the Universe.

This work showed that evaluating voids' influence exclusively is a complicated task, as they are embedded in the large-scale structure. Both under- and overdense regions contribute to the variation of the expansion rate and should be explored in more detail. Future research in this field could potentially investigate the influence of the variety of the overdense structure, providing more insights into the substructure within the voids. Of course, bigger sky surveys might expand our picture of the large-scale structure, revealing new features, such as supervoids.

References

The 2dF Galaxy Redshift Survey. (n.d.). Retrieved from http://www.2dfgrs.net/

Abbott, T. M. C., Abdalla, F. B., Annis, J., Bechtol, K., Blazek, J., Benson, B. A., ... South Pole Telescope Collaboration (2018, November). Dark Energy Survey Year 1 Results: A Precise H_0 Estimate from DES Y1, BAO, and D/H Data. , *480*(3), 3879-3888. doi: 10.1093/mnras/sty1939

Aiola, S., Calabrese, E., Maurin, L., Naess, S., Schmitt, B. L., Abitbol, M. H., ... Zhu, N. (2020, December). The Atacama Cosmology Telescope: DR4 maps and cosmological parameters. , *2020*(12), 047. doi: 10.1088/1475-7516/2020/12/047

Alpher, R. (1999, 01). The big bang model: Its origin and development. *Odessa Astronomical Publications*, *12*, 10-. doi: 10.18524/1810-4215.1999.12.92996

Beeftink, T. (2019). *On the structure, shapes, and alignments of voids* (Bachelor's thesis). University of Groningen, Kapteyn Institute, Groningen.

Blakeslee, J. P., Jensen, J. B., Ma, C.-P., Milne, P. A., & Greene, J. E. (2021, April). The Hubble Constant from Infrared Surface Brightness Fluctuation Distances. , *911*(1), 65. doi: 10.3847/1538-4357/abe86a

Bonvin, V., & Millon, M. (2020, February). *H0licow h0 tension plotting notebook.* Zenodo. Retrieved from https://doi.org/10.5281/zenodo.3635517 doi: 10.5281/zenodo.3635517

Bos, E. G. P., van de Weygaert, R., Dolag, K., & Pettorino, V. (2012, October). The darkness that shaped the void: dark energy and cosmic voids. , *426*(1), 440-461. doi: 10.1111/j.1365-2966.2012.21478.x

Breuval, L., Riess, A. G., Casertano, S., Yuan, W., Macri, L. M., Romaniello, M., ... Soszyński, I. (2024, April). Small Magellanic Cloud Cepheids Observed with the Hubble Space Telescope Provide a New Anchor for the SH0ES Distance Ladder. *arXiv e-prints*, arXiv:2404.08038. doi: 10.48550/arXiv.2404.08038

Cautun, M. (2020). *The dtfe public software.* https://github.com/MariusCautun/DTFE. GitHub.

Cautun, M., van de Weygaert, R., Jones, B. J. T., & Frenk, C. S. (2014, July). Evolution of the cosmic web. , *441*(4), 2923-2973. doi: 10.1093/mnras/stu768

Chincarini, G., & ROOD, H. (1975, 09). Size of the coma cluster. *Nat*, *257*. doi: 10.1038/257294a0

Collaboration, D. N. F. T. I. (n.d.). *Illustris - main.* Retrieved from https://www.illustris-project.org/

Colless, M., Dalton, G., Maddox, S., Sutherland, W., Norberg, P., Cole, S., ... Taylor, K. (2001, December). The 2dF Galaxy Redshift Survey: spectra and redshifts. , *328*(4), 1039-1063. doi: 10.1046/j.1365-8711.2001.04902.x

de Lapparent, V., Geller, M. J., & Huchra, J. P. (1986a, March). A Slice of the Universe. , *302*, L1. doi: 10.1086/184625

de Lapparent, V., Geller, M. J., & Huchra, J. P. (1986b, March). A Slice of the Universe. , *302*, L1. doi: 10.1086/184625

DESI Collaboration, Adame, A. G., Aguilar, J., Ahlen, S., Alam, S., Alexander, D. M., ... Zou, H. (2024, April). DESI 2024 VI: Cosmological Constraints from the Measurements of Baryon Acoustic Oscillations. *arXiv e-prints*, arXiv:2404.03002. doi: 10.48550/arXiv.2404.03002

Di Valentino, E., Mena, O., Pan, S., Visinelli, L., Yang, W., Melchiorri, A., ... Silk, J. (2021, July). In the realm of the Hubble tension-a review of solutions. *Classical and Quantum Gravity*, *38*(15), 153001. doi: 10.1088/1361-6382/ac086d

Einasto, J., Joeveer, M., & Saar, E. (1980, November). Structure of superclusters and supercluster formation. , *193*, 353-375. doi: 10.1093/mnras/193.2.353

Feldbrugge, J. (2021). *Delaunay tesselation field estimator.* https://github.com/jfeldbrugge/DTFE. GitHub.

Fleury, P., Clarkson, C., & Maartens, R. (2017, March). How does the cosmic large-scale structure bias the Hubble diagram? , *2017*(3), 062. doi: 10.1088/1475-7516/2017/03/062

Foster, C., & Nelson, L. A. (2009, June). The size, shape, and orientation of cosmological voids in the sloan digital sky survey. *The Astrophysical Journal*, *699*(2), 1252–1260. Retrieved from http://dx.doi.org/10.1088/0004-637X/699/2/1252 doi: 10.1088/0004-637x/699/2/1252

Freedman, W. L. (2021, September). Measurements of the Hubble Constant: Tensions in Perspective. , *919*(1), 16. doi: 10.3847/1538-4357/ac0e95

Giani, L., Howlett, C., Said, K., Davis, T., & Vagnozzi, S. (2024, January). An effective description of Laniakea: impact on cosmology and the local determination of the Hubble constant. , *2024*(1), 071. doi: 10.1088/1475-7516/2024/01/071

Gregory, S. A., & Thompson, L. A. (1978, June). The Coma/A1367 supercluster and its environs. , *222*, 784-799. doi: 10.1086/156198

Hinshaw, G., Larson, D., Komatsu, E., Spergel, D. N., Bennett, C. L., Dunkley, J., ... Wright, E. L. (2013, September). Nine-year wilkinson microwave anisotropy probe (wmap) observations: Cosmological parameter results. *The Astrophysical Journal Supplement Series*, *208*(2), 19. Retrieved from http://dx.doi.org/10.1088/0067-0049/208/2/19 doi: 10.1088/0067-0049/208/2/19

Hoyle, F., & Vogeley, M. S. (2004, June). Voids in the Two-Degree Field Galaxy Redshift Survey. , *607*(2), 751-764. doi: 10.1086/386279

Huang, C. D., Riess, A. G., Yuan, W., Macri, L. M., Zakamska, N. L., Casertano, S., ... Scolnic, D. (2020, January). Hubble Space Telescope Observations of Mira Variables in the SN Ia Host NGC 1559: An Alternative Candle to Measure the Hubble Constant. , *889*(1), 5. doi: 10.3847/1538-4357/ab5dbd

Hubble, E. (1929, March). A Relation between Distance and Radial Velocity among Extra-Galactic Nebulae. *Proceedings of the National Academy of Science*, *15*(3), 168-173. doi: 10.1073/pnas.15.3.168

International Astronomical Union — IAU. (n.d.). Retrieved from https://www.iau.org/news/pressreleases/detail/iau1812/

Keenan, R. C., Barger, A. J., & Cowie, L. L. (2013, September). Evidence for a ~300 Megaparsec Scale Under-density in the Local Galaxy Distribution. , *775*(1), 62. doi: 10.1088/0004-637X/775/1/62

Kenworthy, W. D., Scolnic, D., & Riess, A. (2019, April). The Local Perspective on the Hubble Tension: Local Structure Does Not Impact Measurement of the Hubble Constant. , *875*(2), 145. doi: 10.3847/1538-4357/ab0ebf

Kirshner, R. P., Oemler, J., A., Schechter, P. L., & Shectman, S. A. (1981, September). A million cubic megaparsec void in Bootes ? , *248*, L57-L60. doi: 10.1086/183623

Kirshner, R. P., Oemler, J., Augustus, Schechter, P. L., & Shectman, S. A. (1987, March). A Survey of the Bootes Void. , *314* , 493. doi: 10.1086/165080

Kugel, R. (2020). *The dynamics of voids and the cosmic web.* University of Groningen, [Unpublished master's thesis].

Li, S., Riess, A. G., Casertano, S., Anand, G. S., Scolnic, D. M., Yuan, W., ... Huang, C. D. (2024, April). Reconnaissance with jwst of the j-region asymptotic giant branch in distance ladder galaxies: From irregular luminosity functions to approximation of the hubble constant. *The Astrophysical Journal*, *966*(1), 20. Retrieved from http://dx.doi.org/10.3847/1538-4357/ad2f2b doi: 10.3847/1538-4357/ad2f2b

Mazurenko, S., Banik, I., Kroupa, P., & Haslbauer, M. (2024, January). A simultaneous solution to the Hubble tension and observed bulk flow within 250 h^{-1} Mpc. , *527*(3), 4388-4396. doi: 10.1093/mnras/stad3357

Nadathur, S., Hotchkiss, S., Diego, J. M., Iliev, I. T., Gottlöber, S., Watson, W. A., & Yepes, G. (2015, June). Self-similarity and universality of void density profiles in simulation and SDSS data. , *449*(4), 3997-4009. doi: 10.1093/mnras/stv513

Pesce, D. W., Braatz, J. A., Reid, M. J., Riess, A. G., Scolnic, D., Condon, J. J., ... Lo, K. Y. (2020, March). The Megamaser Cosmology Project. XIII. Combined Hubble Constant Constraints. , *891*(1), L1. doi: 10.3847/2041-8213/ab75f0

Planck Collaboration, Aghanim, N., Akrami, Y., Ashdown, M., Aumont, J., Baccigalupi, C., ... Zonca, A. (2020, September). Planck 2018 results. VI. Cosmological parameters. , *641*, A6. doi: 10.1051/0004-6361/201833910

Platen, E., van de Weygaert, R., & Jones, B. J. T. (2007, September). A cosmic watershed: the WVF void detection technique. , *380*(2), 551-570. doi: 10.1111/j.1365-2966.2007.12125.x

Riess, A. G., Yuan, W., Macri, L. M., Scolnic, D., Brout, D., Casertano, S., ... Zheng, W. (2022, July). A Comprehensive Measurement of the Local Value of the Hubble Constant with 1 km s^{-1} Mpc^{-1} Uncertainty from the Hubble Space Telescope and the SH0ES Team. , *934*(1), L7. doi: 10.3847/2041-8213/ac5c5b

Ryden, B. (2016). *Introduction to cosmology* (2nd ed.). Cambridge, UK: Cambridge University Press.

Schaap, W. E. (2007). *DTFE: The Delaunay tessellation field estimator* (Unpublished doctoral dissertation). University of Groningen, Netherlands.

Schombert, J., McGaugh, S., & Lelli, F. (2020, August). Using the Baryonic Tully-Fisher Relation to Measure H_o. , *160*(2), 71. doi: 10.3847/1538-3881/ab9d88

Shajib, A. J., Birrer, S., Treu, T., Agnello, A., Buckley-Geer, E. J., Chan, J. H. H., ... Zhang, Y. (2020, June). STRIDES: a 3.9 per cent measurement of the Hubble constant from the strong lens system DES J0408-5354. , *494*(4), 6072-6102. doi: 10.1093/mnras/staa828

Sheth, R. K., & van de Weygaert, R. (2004, May). A hierarchy of voids: much ado about nothing. , *350*(2), 517-538. doi: 10.1111/j.1365-2966.2004.07661.x

Shi, X., & Turner, M. S. (1998, January). Expectations for the Difference between Local and Global Measurements of the Hubble Constant. , *493*(2), 519-522. doi: 10.1086/305169

Tegmark, M., Blanton, M. R., Strauss, M. A., Hoyle, F., Schlegel, D., Scoccimarro, R., ... SDSS Collaboration (2004, May). The Three-Dimensional Power Spectrum of Galaxies from the Sloan Digital Sky Survey. , *606*(2), 702-740. doi: 10.1086/382125

Turner, E. L., Cen, R., & Ostriker, J. P. (1992, May). The Relationship of Local measures of Hubble's Constant to its Global Value. , *103*, 1427. doi: 10.1086/116156

van de Weygaert, R., & Bond, J. R. (2008). Clusters and the Theory of the Cosmic Web. In M. Plionis, O. López-Cruz, & D. Hughes (Eds.), *A pan-chromatic view of clusters of galaxies and the large-scale structure* (Vol. 740, p. 335). doi: 10.1007/978-1-4020-6941-3_10

van de Weygaert, R., & Schaap, W. (2009). The Cosmic Web: Geometric Analysis. In

V. J. Martínez, E. Saar, E. Martínez-González, & M. J. Pons-Bordería (Eds.), *Data analysis in cosmology* (Vol. 665, p. 291-413). doi: 10.1007/978-3-540-44767-2_11

Why do physicists mention "five sigma" in their results? — CERN. (2024, 6). Retrieved from https://home.cern/resources/faqs/five-sigma

Wong, K. C., Suyu, S. H., Chen, G. C. F., Rusu, C. E., Millon, M., Sluse, D., ... Meylan, G. (2020, October). H0LiCOW - XIII. A 2.4 per cent measurement of H_0 from lensed quasars: 5.3σ tension between early- and late-Universe probes. , *498*(1), 1420-1439. doi: 10.1093/mnras/stz3094

Wu, H.-Y., & Huterer, D. (2017, November). Sample variance in the local measurements of the Hubble constant. , *471*(4), 4946-4955. doi: 10.1093/mnras/stx1967